Quantum dot-induced phase stabilization of α-$CsPbI_3$ perovskite for high-efficiency photovoltaics

Authors: Abhishek Swarnkar,[1,2] Ashley R. Marshall,[1,3] Erin M. Sanehira,[1,4] Boris D. Chernomordik,[1] David T. Moore,[1] Jeffrey A. Christians,[1] Tamoghna Chakrabarti[5] and Joseph M. Luther[1*]

Affiliations:

[1] Chemical and Materials Science, National Renewable Energy Laboratory, Golden, CO 80401 USA

[2] Department of Chemistry, Indian Institute of Science Education and Research (IISER), Pune, India – 411008

[3] Department of Chemistry and Biochemistry, University of Colorado, Boulder, CO 80309 USA

[4] Department of Electrical Engineering, University of Washington, Seattle, WA 98195 USA

[5] Metallurgical and Materials Engineering, Colorado School of Mines, Golden, CO 80401 USA

*Corresponding author. Email: joey.luther@nrel.gov

Abstract:

We show nanoscale phase stabilization of $CsPbI_3$ quantum dots (QDs) to low temperatures that can be used as the active component of efficient optoelectronic devices. $CsPbI_3$ is an all-inorganic analog to the hybrid organic cation halide perovskites, but the cubic phase of bulk $CsPbI_3$ (α-$CsPbI_3$) the variant with desirable band gap, is only stable at high temperature. We describe the formation of α-$CsPbI_3$ QD films that are phase stable for months in ambient air. The films support long-range electronic transport, and were used to fabricate colloidal perovskite QD solar cells with an open-circuit voltage of 1.23 volts and efficiency of 10.77 %. These devices also function as light emitting diodes (LEDs) with low turn-on voltage and tunable emission.

One Sentence Summary:

Nanocrystals of the all-inorganic perovskite $CsPbI_3$ impart stability to the cubic crystalline phase, contrary to bulk and thin films, leading to high efficiency quantum dot optoelectronics.

Hybrid organic-inorganic halide perovskites, with the common formulation ABX_3 (where A is an organic cation, B is commonly Pb^{2+}, and X is a halide), were first applied to PVs as methylammonium lead triiodide ($CH_3NH_3PbI_3$) in 2009 (*1*). Perovskite PV devices processed from solution inks now convert >22% of incident sunlight into electricity, on par with the best thin film chalcogenide and silicon devices, but durability of the semiconductor presents a major technical hurdle to commercialization. Under environmental stress, $CH_3NH_3PbI_3$ dissociates into PbI_2 and CH_3NH_3I, the latter of which is volatile (*2*).

Thus, an all-inorganic structure without a volatile organic component is highly desired. The all-inorganic Pb-halide perovskite with the most appropriate band gap for PV is cubic (α) $CsPbI_3$ (E_g=1.73 eV) because geometrical constraints of the perovskite structure require a large +1 A-site cation, and Cs is the most feasible. However, below 320°C, the orthorhombic (δ) phase (E_g=2.82 eV) is thermodynamically preferred (*3*). Nevertheless, groups have explored $CsPbX_3$ compounds as PV materials, but films of α-$CsPbI_3$ undergo immediate transformation to the orthorhombic phase when exposed to ambient conditions (*4*). Attempts to stabilize the cubic phase through alloying with Br^-, $CsPbIBr_2$ shows a much reduced δ to α phase transition temperature of 100 °C(*3*). However, the composition change leads to an undesired increase in the band gap. We show that nanocrystal surfaces can be used to stabilize α-$CsPbI_3$ at room temperature, far below the phase transition temperature for thin film or bulk materials. We further show that we can control the electronic coupling of quantum dots (QDs) to produce air-stable, efficient solar cells (initial efficiency above 10%) based on this all-inorganic material.

Many physical properties differ between nanometer-sized and bulk crystalline materials of the same chemical compound. One such example is the structural phase in which the

constituent atoms are arranged. For example, the semiconductors CdS and CdSe embody a rock salt structure at high pressure. However, the solid-solid phase transition point between the rock salt phase and the hexagonal wurtzite phase can vary greatly in temperature and pressure as a function of crystal size (*5, 6*). Manipulated size-dependent phase diagrams have been explored in a variety of material systems with advantageous properties of the crystals emerging at reduced dimensions in oxides (*e.g.,* TiO_2), lanthanides (*e.g.,* $NaYF_4$)(*7*), metals (*e.g.,* Ag)(*8*), and ferroelectrics (*e.g.,* the perovskite $BaTiO_3$)(*9*).

Synthetic protocols of colloidal halide perovskite QDs have recently been reported (*10-17*). $CsPbX_3$ QDs exhibit improved room temperature cubic phase stability and attractive optical properties for a wide range of applications(*11, 18-22*). Experiments on size and shape dependent optical properties (*11, 23-25*), surface chemistry(*26*), and other photophysics(*27*) are being explored for $CsPbBr_3$ QDs. However, previous studies were unable to achieve cubic $CsPbI_3$ QDs that were stable enough to extensively characterize.

We present an improved synthetic route and purification approach to $CsPbI_3$ QDs. Once purified, the QDs retain the cubic phase for months in ambient air and even at cryogenic temperatures. A method for perovskite QD film assembly is described that allows for efficient dot-to-dot electronic transport while retaining the phase stability of the individual QDs. The PV cells produced from this approach have the highest efficiency and stabilized power output of any all-inorganic perovskite absorber, produce 1.23 V at open circuit (among the best of any perovskite PV), and also function as light-emitting diodes (LEDs), emitting visible red light with low turn-on voltage.

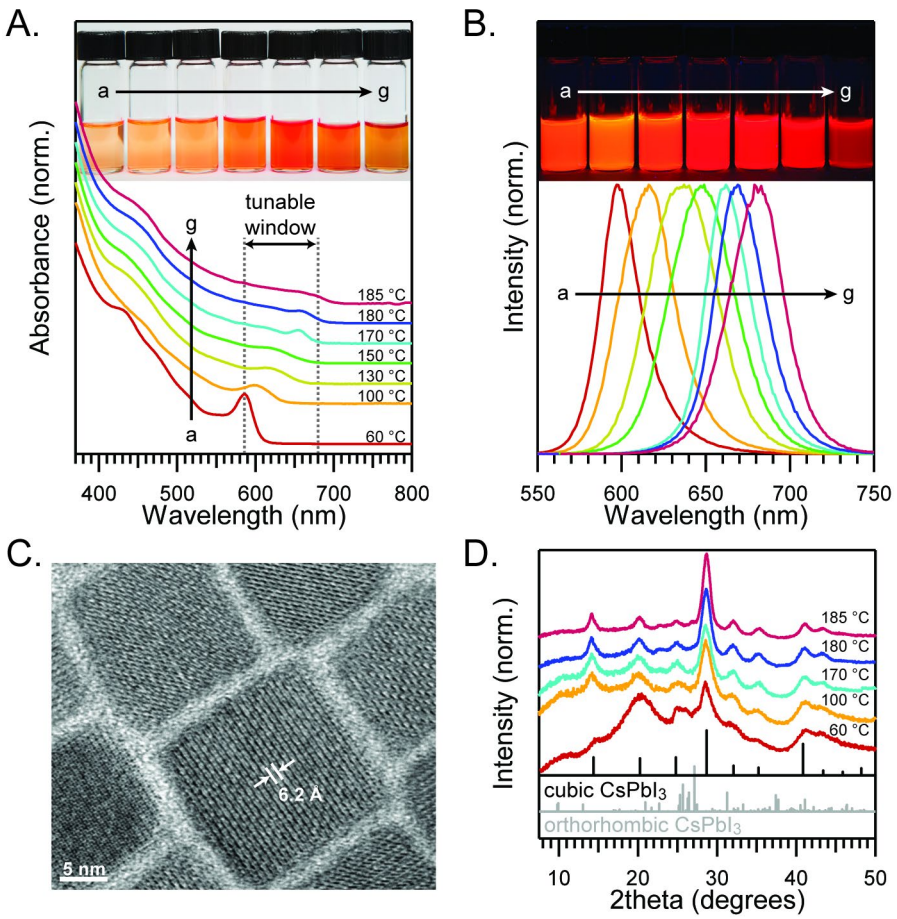

Fig. 1. Characterization of $CsPbI_3$ QDs. (**A**) Ultraviolet-visible (UV-vis) absorption spectra and photographs of $CsPbI_3$ QDs synthesized at (a) 60 (3.4 nm), (b) 100 (4.5 nm), (c) 130 (5 nm), (d) 150 (6.8 nm), (e) 170 (8 nm), (f) 180 (9 nm), (g) 185 °C (12.5 nm), average size from TEM shown in parentheses. (**B**) Normalized photoluminescence spectra and photographs under UV illumination of the QDs from (A). (**C**) High-resolution transmission electron micrograph (HRTEM) of $CsPbI_3$ QDs synthesized at 180 °C. (**D**) XRD patterns of QDs synthesized at (from bottom to top) 60, 100, 170, 180, and 185 °C confirming that they crystallize in the cubic phase of $CsPbI_3$.

Figure 1 shows the tunability of the band gap via quantum confinement, in a series of $CsPbI_3$ QDs synthesized by the addition of Cs-oleate to a flask containing PbI_2 precursor, as first described by Protesescu et al.(*11*), here using injection temperatures between 60 and 185 °C to control the size (*28*). This produces QDs solubilized by non-crystalline iodide and oleylammonium surface ligands (*26*). Similar to previous reports(*29, 30*), we find that unpurified QDs transform to the orthorhombic phase within several days [fig. S1 (*28*)]. However, we developed a process to isolate the QDs utilizing methyl acetate (MeOAc), an antisolvent that

removes excess unreacted precursor without inducing agglomeration. Using this extraction procedure we find the QDs are stable in the cubic phase for months with ambient storage.

The excitonic peak of $CsPbI_3$ shifted between 585 and 670 nm corresponding to QD sizes between 3 and 12.5 nm. The corresponding normalized PL spectra of the samples are shown in Fig. 1B, along with a photograph of the QDs in hexane. Upon ultraviolet (UV) excitation, emission was in the orange (600 nm) to red (680 nm) color range corresponding to a band gap between 2.07 and 1.82 eV [photographs showing PL from dried QD powders are shown in fig. S2 (*28*)]. The full-width at half-maximum of the PL for the smallest QDs was 83 meV, and increased slightly for the larger sizes, while the PL quantum yield varied from 21 to 55% for different sizes [fig. S3 (*28*)].

In contrast to the unstable cubic phase of bulk $CsPbI_3$ at room temperature, QDs have been reported to retain the cubic phase because of the large contribution of surface energy (*11, 31*) (Fig. 1D). The softer basic nature of I^- compared to Br^- results in weaker acid-base interactions between the halide and the oleylammonium ligand (a hard acid) in the case of $CsPbI_3$, compared to $CsPbBr_3$(*30, 32*). Therefore, the isolation of $CsPbI_3$ QDs is more difficult than that of $CsPbBr_3$ QDs because of the loss of ligand during extraction, causing agglomeration and reversion to the orthorhombic phase. Thus we find that MeOAc, which isolates the QDs without full removal of the surface species, is critical to the phase-stable devices described below.

The high-resolution transmission electron micrograph (TEM) of the sample synthesized at 180 °C (Fig. 1C) shows an interplanar distance of 0.62 nm, consistent with the (100) plane of cubic phase $CsPbI_3$(*24, 31, 33*). In Fig. 2, A and B, powder XRD patterns and UV-visible absorption spectra confirm the absence of diffraction peaks or the high energy (~3 eV) sharp

absorption characteristic of orthorhombic phase formation(*31*), even after 60 days of storage in ambient. Additionally, the QDs remained in the cubic phase even after the solution was cooled to 77 K, further demonstrating the expanded temperature stability of the cubic phase.

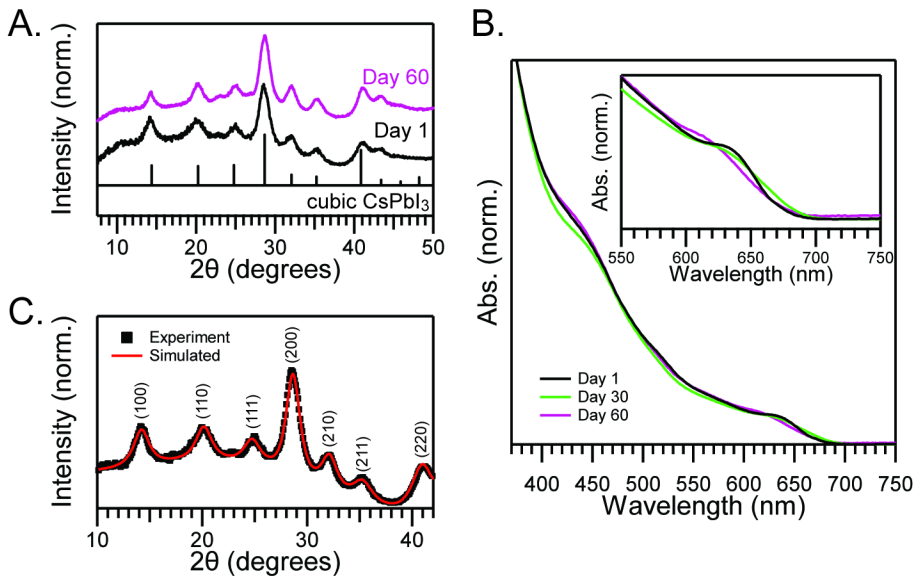

Fig. 2. Phase Stability of $CsPbI_3$ QDs. (**A**) Powder XRD patterns and (**B**) UV-Visible absorption spectra, normalized at 370 nm, of $CsPbI_3$ QDs synthesized at 170 °C and stored in ambient conditions for a period of 60 days. Inset shows the slight blue shift that is seen in the excitonic peak with extended storage. (**C**) Rietveld refinement fitting of $CsPbI_3$ NC XRD pattern revealing pure cubic phase $CsPbI_3$.

Rietveld refinement of the XRD patterns [Fig. 2C and described in the SM (*28, 35, 36*)] allowed us to quantify the contribution from cubic and orthorhombic phases. No detectable orthorhombic phase was found. Additionally, lattice parameters of three different size $CsPbI_3$ QD samples were estimated (Table 1). The lattice parameter values showed a size dependence and are lower than the previously measured experimental value (6.2894 Å at 634 K) of bulk cubic $CsPbI_3$ (*31*). Our measurements were performed at 273 K, whereas high temperatures are required to characterize bulk cubic $CsPbI_3$. A similar increase in lattice parameter with decreasing particle size has been reported in other systems and attributed to electrostatic relaxation with decreasing crystal size(*34*).

Table 1. Results of the Rietveld refinement.

QD Size (TEM)	QD Size (Rietveld)	a (Å)	R_{wp}
8 nm	9 ± 1 nm	6.231 ± 0.002	3.42
9 nm	10 ± 1 nm	6.220 ± 0.002	6.50
15.5 nm	17 ± 2 nm	6.189 ± 0.002	7.79

In order to use this highly phase-stable α-$CsPbI_3$ QDs in optoelectronic devices, we developed a method to cast electronically conductive NC films. The QDs were first spin-cast from octane, then dipped in a saturated MeOAc solution of either $Pb(OAc)_2$ or $Pb(NO_3)_2$ (neat MeOAc was used as a control). This process was repeated multiple times, typically 3 to 5, to produce NC films with thicknesses between 100 and 400 nm. The optical absorption and PL spectra (Fig 3A, for three samples with indicated reaction temperature) show that in each case, the film absorbance and PL was red-shifted ~20 nm from that of the QDs in solution, while the tunable emission properties of the films indicate that quantum confinement is preserved. Fourier-transform infrared (FTIR) spectra show the removal of organic ligands from the film with exposure to neat MeOAc (Fig. 3B) given the near absence of C-H modes near 3000 cm^{-1} or below ~2000 cm^{-1} belonging to oleylammonium, oleate, or octadecene. We therefore attribute the preserved phase stability of the QDs in the films to the size of the crystals (given the quantum confined optical properties) independent of the surface species.

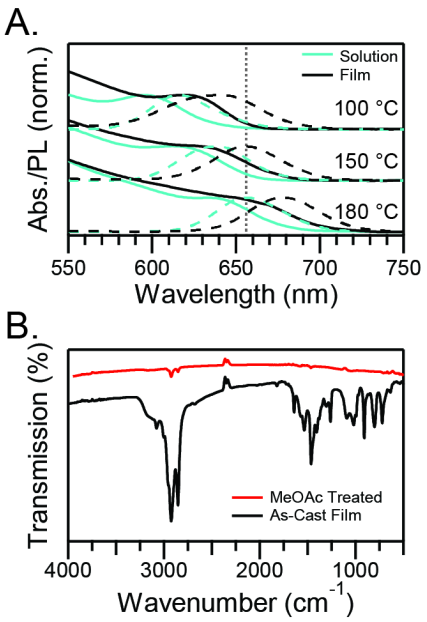

Fig. 3. $CsPbI_3$ QD Films. (**A**) UV-vis absorption (solid lines) and PL spectra (dashed lines) of $CsPbI_3$ QDs in solution (blue) and cast as films (black) for QDs synthesized at 100, 150, and 180 °C. (**B**) FTIR spectra showing the IR transmission of a $CsPbI_3$ QD film as cast (black) and after treating with MeOAc (red).

We also probed the interaction of Pb^{2+} salts with QDs in solution and on films by monitoring the fluorescence [fig. S4 (*28*)]. Titration of a small amount of $Pb(OAc)_2$ to the NC solution showed an enhancement in PL, suggesting improved surface passivation. Titrations with only MeOAc caused fast PL quenching. Similarly, dip-coating of the NC film in a saturated solution of $Pb(OAc)_2$ in MeOAc resulted in a PL enhancement of ~350% compared to dip-coating in MeOAc alone.

We fabricated PV cells with these $CsPbI_3$ QDs films as the photoactive material. A schematic of device architecture is shown in Fig. 4A, and scanning electron micrograph cross-section image is shown in Fig. 4B. The reverse scan current density-voltage (*JV*) curves showed an open-circuit voltage (V_{OC}) of 1.23 V, and 10.77% power conversion efficiency (PCE) for a 0.10 cm^2 cell made and tested completely in ambient conditions (relative humidity ~15 to 25%)] (Fig. 4C). Furthermore, the PCE improved from its initial value over the course of 15 days

storage in dry but ambient conditions [also see fig S5 (*28*)]. In fig. S6 (*28*), we show the stabilized power output of the cell by measuring the current density while the device is biased at 0.92 V. In Fig. 4D, the spectral response of the solar cell is shown, indicating a bandgap of 1.75 eV for this film. Both, the *JV*-scan efficiency and stabilized power output (SPO) for these QD devices shows promise over conventional all-inorganic perovskites which have thus far been reported at 9.8% with SPO of 5.6% (*4, 31, 35*). Additionally, previous reports indicate that $CsPbI_3$ devices must be fabricated and measured in nitrogen dry boxes(*4*). The V_{OC} is much higher than for other QD solar cells [typically < 0.7 V], and among the highest V_{OC} in all perovskite PV cells for band gaps below 2 eV. We note that we have not optimized the device architecture nor the NC film treatment scheme. We find that dip-coating spin-cast films in neat MeOAc, and MeOAc saturated with $Pb(OAc)_2$ or $Pb(NO_3)_2$ all work reasonably well (*JV*-scanned PCE > 9%) in PV devices.

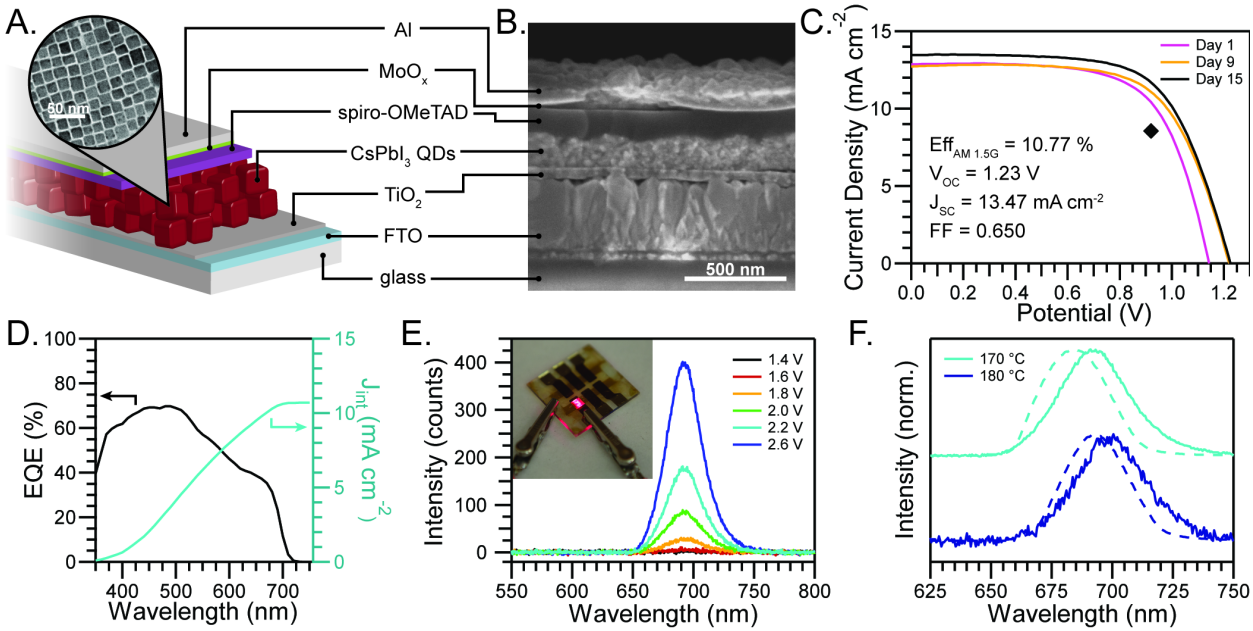

Fig. 4. $CsPbI_3$ optoelectronic Devices. (**A**) Schematic (with HRTEM image of QDs) and (**B**) SEM cross-section of the $CsPbI_3$ solar cells. (**C**) Current-voltage curves of a device measured in air over the course of 15 days. The black diamond represents the stabilized output of the device at 0.92 V, as shown in fig. S6. (**D**) External quantum efficiency (black, left ordinate) and integrated current density (blue, right ordinate) of the device. (**E**) EL spectra of $CsPbI_3$ solar cell ($CsPbI_3$ synthesized at 170 °C) under forward bias. The inset shows a photograph of the luminescent device. (**F**) PL (dotted lines) and EL (solid lines) spectra of

completed devices fabricated using $CsPbI_3$ QDs synthesized at 170 and 180 °C demonstrating size quantization effects in the completed devices.

Given the PL properties of these perovskite QDs, we were explored their use as LEDs. The PV devices also produced visible electroluminescence (EL) when biased above V_{OC}. The EL had a low turn-on voltage near the bandgap of the $CsPbI_3$ with increasing intensity at larger applied biases (Fig. 4E). These spectra provide direct evidence that quantum confinement is retained in the complete devices, critical to retaining the improved cubic phase stability, as seen by the shift in both the EL and PL spectra of devices with different size QDs (Fig. 4F). The synthesis of normally unstable material phases stabilized through colloidal QD synthesis provides another mechanism for materials design for photovoltaics, LEDs, and other applications.

Supplementary Materials:

Materials and Methods

Figs. S1 to S6

References (*36, 37*)

References:

1. A. Kojima, K. Teshima, Y. Shirai, T. Miyasaka, Organometal Halide Perovskites as Visible-Light Sensitizers for Photovoltaic Cells. *Journal of the American Chemical Society* **131**, 6050 (2009/05/06, 2009).
2. D. P. Nenon *et al.*, Structural and chemical evolution of methylammonium lead halide perovskites during thermal processing from solution. *Energy & Environmental Science*, (2016).
3. S. Sharma, N. Weiden, A. Weiss, in *Zeitschrift für Physikalische Chemie*. (1992), vol. 175, pp. 63.
4. R. E. Beal *et al.*, Cesium Lead Halide Perovskites with Improved Stability for Tandem Solar Cells. *The Journal of Physical Chemistry Letters* **7**, 746 (2016/03/03, 2016).
5. A. P. Alivisatos, Semiconductor Clusters, Nanocrystals, and Quantum Dots. *Science* **271**, 933 (1996-02-16 00:00:00, 1996).
6. S. H. Tolbert, A. P. Alivisatos, Size Dependence of a First Order Solid-Solid Phase Transition: The Wurtzite to Rock Salt Transformation in CdSe Nanocrystals. *Science* **265**, 373 (1994-07-15 00:00:00, 1994).
7. F. Wang *et al.*, Simultaneous phase and size control of upconversion nanocrystals through lanthanide doping. *Nature* **463**, 1061 (02/25/print, 2010).
8. C. C. Yang, S. Li, Size-Dependent Phase Stability of Silver Nanocrystals. *The Journal of Physical Chemistry C* **112**, 16400 (2008/10/23, 2008).
9. S. Schlag, H. F. Eicke, Size driven phase transition in nanocrystalline BaTiO3. *Solid State Communications* **91**, 883 (1994).
10. L. C. Schmidt *et al.*, Nontemplate Synthesis of CH3NH3PbBr3 Perovskite Nanoparticles. *Journal of the American Chemical Society* **136**, 850 (Jan, 2014).
11. L. Protesescu *et al.*, Nanocrystals of Cesium Lead Halide Perovskites (CsPbX3, X = Cl, Br, and I): Novel Optoelectronic Materials Showing Bright Emission with Wide Color Gamut. *Nano Letters* **15**, 3692 (Jun, 2015).
12. F. Zhang *et al.*, Brightly Luminescent and Color-Tunable Colloidal CH3NH3PbX3 (X = Br, I, Cl) Quantum Dots: Potential Alternatives for Display Technology. *ACS Nano* **9**, 4533 (Apr, 2015).
13. D. D. Zhang, S. W. Eaton, Y. Yu, L. T. Dou, P. D. Yang, Solution-Phase Synthesis of Cesium Lead Halide Perovskite Nanowires. *Journal of the American Chemical Society* **137**, 9230 (Jul, 2015).
14. H. Huang *et al.*, Emulsion Synthesis of Size-Tunable CH3NH3PbBr3 Quantum Dots: An Alternative Route toward Efficient Light-Emitting Diodes. *ACS Applied Materials & Interfaces* **7**, 28128 (2015/12/30, 2015).
15. Y. Hassan *et al.*, Structure-Tuned Lead Halide Perovskite Nanocrystals. *Adv. Mater.* **28**, 566 (Jan, 2016).

16. S. Sun, D. Yuan, Y. Xu, A. Wang, Z. Deng, Ligand-Mediated Synthesis of Shape-Controlled Cesium Lead Halide Perovskite Nanocrystals via Reprecipitation Process at Room Temperature. *ACS Nano*, (2016/02/17, 2016).

17. T. C. Jellicoe *et al.*, Synthesis and Optical Properties of Lead-Free Cesium Tin Halide Perovskite Nanocrystals. *Journal of the American Chemical Society* **138**, 2941 (2016/03/09, 2016).

18. Y. Wang *et al.*, All-Inorganic Colloidal Perovskite Quantum Dots: A New Class of Lasing Materials with Favorable Characteristics. *Adv. Mater.* **27**, 7101 (2015).

19. S. Yakunin *et al.*, Low-threshold amplified spontaneous emission and lasing from colloidal nanocrystals of caesium lead halide perovskites. *Nat. Commun.* **6**, (Aug, 2015).

20. Y. Xu *et al.*, Two-Photon-Pumped Perovskite Semiconductor Nanocrystal Lasers. *Journal of the American Chemical Society*, (2016/03/03, 2016).

21. A. Swarnkar *et al.*, Colloidal CsPbBr3 Perovskite Nanocrystals: Luminescence beyond Traditional Quantum Dots. *Angew. Chem.-Int. Edit.* **54**, 15424 (Dec, 2015).

22. F. Hu *et al.*, Superior Optical Properties of Perovskite Nanocrystals as Single Photon Emitters. *ACS Nano* **9**, 12410 (2015/12/22, 2015).

23. Q. A. Akkerman *et al.*, Solution Synthesis Approach to Colloidal Cesium Lead Halide Perovskite Nanoplatelets with Monolayer-Level Thickness Control. *Journal of the American Chemical Society* **138**, 1010 (2016/01/27, 2016).

24. N. S. Makarov *et al.*, Spectral and Dynamical Properties of Single Excitons, Biexcitons, and Trions in Cesium–Lead-Halide Perovskite Quantum Dots. *Nano Letters*, (2016/02/16, 2016).

25. Y. Bekenstein, B. A. Koscher, S. W. Eaton, P. Yang, A. P. Alivisatos, Highly Luminescent Colloidal Nanoplates of Perovskite Cesium Lead Halide and Their Oriented Assemblies. *Journal of the American Chemical Society* **137**, 16008 (2015/12/30, 2015).

26. J. De Roo *et al.*, Highly Dynamic Ligand Binding and Light Absorption Coefficient of Cesium Lead Bromide Perovskite Nanocrystals. *ACS Nano* **10**, 2071 (2016/02/23, 2016).

27. Y. S. Park, S. J. Guo, N. S. Makarov, V. I. Klimov, Room Temperature Single-Photon Emission from Individual Perovskite Quantum Dots. *ACS Nano* **9**, 10386 (Oct, 2015).

28. See the supplementary materials on *Science*, (Online).

29. C. C. Lin, A. Meijerink, R.-S. Liu, Critical Red Components for Next-Generation White LEDs. *The Journal of Physical Chemistry Letters* **7**, 495 (2016/02/04, 2016).

30. Q. A. Akkerman *et al.*, Tuning the Optical Properties of Cesium Lead Halide Perovskite Nanocrystals by Anion Exchange Reactions. *Journal of the American Chemical Society* **137**, 10276 (Aug, 2015).

31. G. E. Eperon *et al.*, Inorganic caesium lead iodide perovskite solar cells. *Journal of Materials Chemistry A* **3**, 19688 (2015).

32. R. G. Pearson, Hard and Soft Acids and Bases. *Journal of the American Chemical Society* **85**, 3533 (1963/11/01, 1963).

33. D. M. Trots, S. V. Myagkota, High-temperature structural evolution of caesium and rubidium triiodoplumbates. *Journal of Physics and Chemistry of Solids* **69**, 2520 (10//, 2008).

34. S. Tsunekawa, K. Ishikawa, Z. Q. Li, Y. Kawazoe, A. Kasuya, Origin of Anomalous Lattice Expansion in Oxide Nanoparticles. *Physical Review Letters* **85**, 3440 (10/16/, 2000).

35. R. J. Sutton *et al.*, Bandgap-Tunable Cesium Lead Halide Perovskites with High Thermal Stability for Efficient Solar Cells. *Advanced Energy Materials* **6**, n/a (2016).

36. L. Lutterotti, MAUD, version 2.55 released April 30, 2015, http://www.ing.unitn.it/~luttero/maud.

37. L. Lutterotti, P. Scardi, P. Maistrelli, LSI-a computer program for simultaneous refinement of material structure and microstructure. *Journal of applied crystallography* **25**, 459 (1992).

Acknowledgments:

We thank Jao van de Lagemaat, William Tumas, Hyekyoung Choi, Matthew Beard, and Joseph Berry for helpful discussions and Bobby To for SEM imaging. We acknowledge support from the Center for Advanced Solar Photophysics (CASP), an Energy Frontier Research Center funded by the US Department of Energy, Office of Science, Office of Basic Energy Sciences for quantum dot coupling and solar cell structures. Device durability and structural phase characterization is performed within the hybrid perovskite solar cell program of the National Center for Photovoltaics funded by the U.S. Department of Energy, Office of Energy Efficiency and Renewable Energy, Solar Energy Technologies Office under contract number DE-AC36-08GO28308DOE. The original conception and QD synthesis was performed under the Laboratory Directed Research and Development program at NREL. A. S. acknowledges the Bhaskara Advanced Solar Energy (BASE) fellowship funded by Department of Science and Technology, Gov. of India and Indo-US Science and Technology Forum (IUSSTF). E. M. S.

acknowledges a NASA Space Technology Research Fellowship. D. T. M. acknowledges the NREL Director's Fellowship.